Research Article

Nano Research
2022, 15(6): 4996–5003

ISSN 1998-0124 CN 11-5974/O4
https://doi.org/10.1007/s12274-022-4158-0

Dislocation-strained MoS_2 nanosheets for high-efficiency hydrogen evolution reaction

Shihao Wang[1,§], Longlu Wang[1,§] (✉), Lingbin Xie[2], Weiwei Zhao[2], Xia Liu[3] (✉), Zechao Zhuang[4], YanLing Zhuang[1], Jing Chen[1], Shujuan Liu[2], and Qiang Zhao[1,2] (✉)

[1] *College of Electronic and Optical Engineering, Nanjing University of Posts and Telecommunications, Nanjing 210023, China*
[2] *Key Laboratory for Organic Electronics and Information Displays and Jiangsu Key Laboratory for Biosensors, Institute of Advanced Materials (IAM) and Institute of Flexible Electronics (Future Technology), Nanjing University of Posts and Telecommunications, Nanjing 210023, China*
[3] *College of Chemistry and Chemical Engineering, Qingdao University, Qingdao 266071, China*
[4] *Department of Chemistry, Tsinghua University, Beijing 100084, China*
[§] *Shihao Wang and Longlu Wang contributed equally to this work.*

Received: 19 December 2021 / **Revised:** 12 January 2022 / **Accepted:** 13 January 2022

ABSTRACT

Defect engineering is one of the effective strategies to optimize the physical and chemical properties of molybdenum disulfide (MoS_2) to improve catalytic hydrogen evolution reaction (HER) performance. Dislocations, as a typical defect structure, are worthy of further investigation due to the versatility and sophistication of structures and the influence of local strain effects on the catalytic performance. Herein, this study adopted a low-temperature hydrothermal synthesis strategy to introduce numerous dislocation-strained structures into the in-plane and out-of-plane of MoS_2 nanosheets. Superior HER catalytic activity of 5.85 $mmol \cdot g^{-1} \cdot h^{-1}$ under visible light was achieved based on the high-density dislocations and the corresponding strain field. This work paves a new pathway for improving the catalytic activity of MoS_2 via a dislocation-strained synergistic modulation strategy.

KEYWORDS

molybdenum disulfide, dislocation, strain, hydrogen evolution reaction

1 Introduction

In recent years, among the non-Pt-based catalysts, the layered transition metal dichalcogenides (TMDs) nanomaterials with MoS_2 as representatives are considered as promising candidates for HER catalyst [1, 2]. Defect engineering has been widely used to optimize the HER catalytic activity of MoS_2 [3–11]. Dislocations, as a special type of defects, are considered as attractive design targets for heterogeneous catalysis because they are stable under many catalysis-related conditions and will produce a large amount of disturbance when they intersect with the surface [12–18].

Recently, researchers have been committed to improving the inherent catalytic performance of MoS_2 by dislocation engineering. Wang et al. systematically evaluated various structural defects on the base plane of MoS_2. The Gibbs free energy calculated by first-principles demonstrated that the HER catalytic efficiency of MoS_2 could be greatly improved by introducing dislocation into MoS_2 domains [19]. Subsequently, Liu et al. grew wafer-level atomic thin-film TMD with ultra-high-density grain boundaries (GBs) on SiO_2 substrate, showing favorable HER performance and proving the inherent high excitation activity of TMD GBs [20]. Nevertheless, this approach is only effective for flat MoS_2 catalysts due to the substrate used and is thus unsuitable for large-scale synthesis. In the previous studies, it has been demonstrated that the dislocation with internal strain could trigger the catalyst surface deformation by bulge or depression [21–25]. It inspires us to design the high-density dislocation with strong strain on MoS_2 for high-performance HER. On one hand, engineering the dislocation with the strain effect could fine-tune the electronic structure of the active site by moving the d-band center of the S atom down to the Fermi level, which allows ΔG_{H^*} close to zero, thus improving the HER performance [26–30]. On the other hand, the resulting stacking fault can connect interlayers and provide an electron transfer network to ensure the vertical conductivity for better HER activity [31–33]. Given this, designing high-density dislocation is an effective method to realize the high-efficiency HER performance of MoS_2 catalysts. However, it remains a grand challenge to synthesize high-density dislocation of MoS_2 nanosheets with strain in realistic HER application.

In this work, a combination of *ex-situ* high-resolution transmission electron microscopy (HRTEM) and geometric phase analysis (GPA) was used to study the in- and out-of-plane dislocation and strain distribution of MoS_2 nanosheets. Density functional theory (DFT) results revealed that exploring dislocations on the MoS_2 nanostructures could adjust the electronic structure and optimize hydrogen adsorption free energy (ΔG_{H^*}) close to zero. The dislocation-strained MoS_2 nanosheets had high-density active sites, low charge transfer resistance, and excellent stability when they were used as HER catalysts. The dislocation-strained MoS_2 (D-S-MoS_2) prepared by the low-temperature hydrothermal method opens up a new way for the design of high-efficiency MoS_2 based HER catalysts.

Address correspondence to Longlu Wang, wanglonglu@njupt.edu.cn; Xia Liu, Liux918@163.com; Qiang Zhao, iamqzhao@njupt.edu.cn

2 Results and discussion

Dislocations are usually composed of different structural motifs, including the arrangement of pentagon–heptagon cores (5|7), quadrilateral–hexagon cores (4|6), hexagon–octagon cores (6|8), and quadrilateral–octagon cores (4|8) [34–37]. Among them, 5|7 core is easier to acquire in the experiment due to its lower formation energy and smaller Burgers vector [35, 38, 39]. The electronic properties of MoS_2 with 5|7 dislocation cores were calculated, as shown in Fig. 1. DFT calculations of the band structure in Fig. 1(a) suggest that when the 5|7 dislocation core is formed, the bandgap is significantly narrower than that of the original defect-free 2H-MoS_2 (from 1.670 eV to 1.302 eV), accompanied by the generation of defect energy levels. These drastic changes indicate that dislocation has a significant influence on the electronic structure of MoS_2. The dislocation energy level can change the current orbital energy level, i.e., to reduce the transition energy from valence band (VB) to conduction band (CB) and significantly improve the electron transferability. Locally increased electron affinity can attract protons [40]. These partially negative charges caused by dislocation can greatly promote the capture of positively charged H species. The visualized highest occupied molecular orbitals (HUMOs) and lowest unoccupied molecular orbitals (LUMOs) intuitively reveal the electron transfer of MoS_2 with dislocation defects. As shown in Figs. 1(b) and 1(c), the charge is mainly concentrated around the 5|7 dislocation core, indicating its predominant electron transferability. The generation of dislocation would increase the affinity of the original inert base with less catalytic activity to electrons, making it easier to capture the positively charged H.

Under the guidance of theoretical calculation, MoS_2 nanosheets with high-density dislocations were synthesized by the low-temperature hydrothermal method, and the 5|7 dislocation core structure was also observed by HRTEM characterization (Fig. S1 in the Electronic Supplementary Material (ESM)). Generally, in the traditional high-temperature hydrothermal synthesis process, the reaction is sufficient to form MoS_2 nanosheets with higher crystallinity and fewer defects [41]. To introduce dislocation defects, a long-term low-temperature hydrothermal reaction (an improved one-pot hydrothermal method) was used to make the dislocations trapped in the crystal by lattice distortion and kinetics [42].

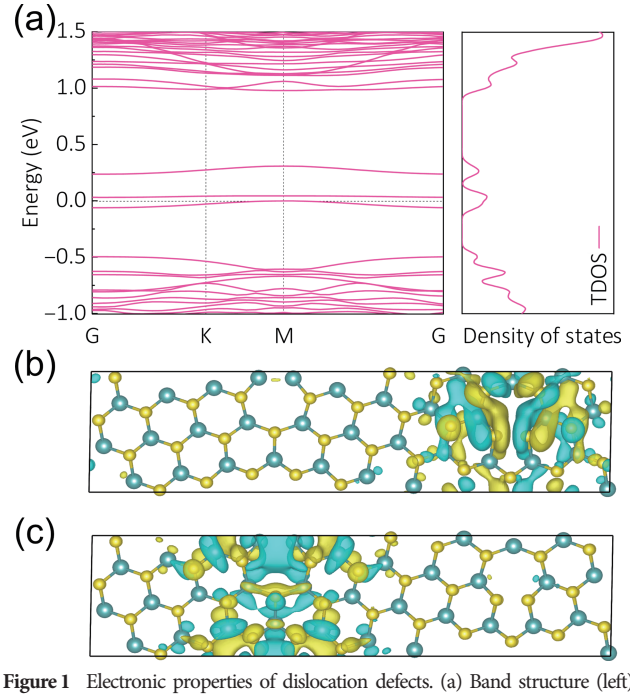

Figure 1 Electronic properties of dislocation defects. (a) Band structure (left) and density of states (DOS, right) of MoS_2 with 5|7 dislocation core. (b) and (c) Visualization of HUMO–LUMO energy level structure.

The formation process of D-S-MoS_2 is displayed in Fig. 2(a). MoS_2 nanoflowers with high-density dislocations can be prepared by low-temperature hydrothermal treatment for 10 days with ammonium molybdate tetrahydrate ($(NH_4)_6Mo_7O_{24}{\cdot}4H_2O$) and high concentration thiourea (CH_4N_2S) as precursors. Figure 2(b) illustrates the formation mechanism of D-S-MoS_2. It is considered to mainly include two steps: (1) vulcanization of low-valent oxide materials to form clusters (MoS_x) and (2) the splicing and combination of clusters in solution to form MoS_2 nanostructures. Compared with high-temperature conditions, the molecular reconstruction is not violent enough, and many cluster structures (Mo_3S_{13} and Mo_2S_{12}) will be produced due to the long-term and low-temperature hydrothermal synthesis of D-S-MoS_2 [43]. The $[Mo_7O_{24}]^{2-}$ decomposed by $(NH_4)_6Mo_7O_{24}{\cdot}4H_2O$ results in two different vulcanization products under the influence of a high concentration sulfur source, one is $[Mo_3S_{13}]^{2-}$ and the other is $[Mo_2S_{12}]^{2-}$. During the 10 days hydrothermal reaction at a low temperature, the clusters splice disorderly and gradually form weakly crystalline MoS_2 nanosheets, which exhibit short-range ordering [44–46] and relatively low crystallinity, porous structure, and a large number of dislocations (in-plane and out-of-plane). The products in different stages of the improved one-pot hydrothermal synthesis process were analyzed and compared to verify the accuracy of the synthesis mechanism. After low-temperature hydrothermal reaction for 12 h, the solution changes from clear to light brick red, and there is an obvious tinter phenomenon. The transmission electron microscope (TEM) image display that most of the products are presented in the form of MoS_x cluster quantum dots (Fig. S2 in the ESM). Subsequently, the low-temperature hydrothermal time is increased to observe the changes in the morphology of the product during the reaction (Fig. S3 in the ESM). The fragmented products (Fig. S3(a) in the ESM) are gradually spliced and finally combined into a D-S-MoS_2 nanoflower after a longer reaction time (Fig. S3(d) in the ESM). The crystal structure of MoS_2 under low temperature hydrothermal conditions for 6, 8 and 10 days was measured by powder X-ray diffraction (XRD) (Fig. S4 in the ESM). The results indicate that the samples after low-temperature hydrothermal synthesis for 10 days have obvious MoS_2 characteristic peaks, which is consistent with the previously reported results. Furthermore, *in situ* electron spin-resonance spectroscopy (ESR) indicates that the defect density increases significantly after low-temperature hydrothermal treatment (Fig. S5 in the ESM). The HRTEM and corresponding energy-dispersive X-ray spectroscopy (EDX) elemental mapping images (Fig. 2(c) and Fig. S6 in the ESM) demonstrate that only Mo and S are evenly distributed throughout the completely distorted nanosheet, thus confirming the formation of D-S-MoS_2.

The nano-scale strain caused by dislocation on the surface of the MoS_2 substrate was further determined by HRTEM and GPA [47, 48]. Figure 3(a) exhibits an HRTEM image of D-S-MoS_2 nanosheets attached to a carbon film. The difference in the stacking thickness of the nanosheets separates the carbon film (brighter) and D-S-MoS_2 nanosheets (darker) According to the fast Fourier transform (FFT) results in the insert of Fig. 3(a), the $d_{(100)}$ and $d_{(101)}$ spacings of MoS_2 nanosheets are about 0.265 and 0.255 nm. Compared with the standard PDF card of MoS_2 (JCPDS Card No. 73-1508), the lattice spacings are compressed by 3% and 4% respectively. As exhibited in Fig. 3(b), FFT transform filtering was performed on the yellow dotted line box in Fig. 3(a) to obtain a clear D-S-MoS_2 in-plane image. It is observed that the synthesized MoS_2 base surface displays a shape similar to the

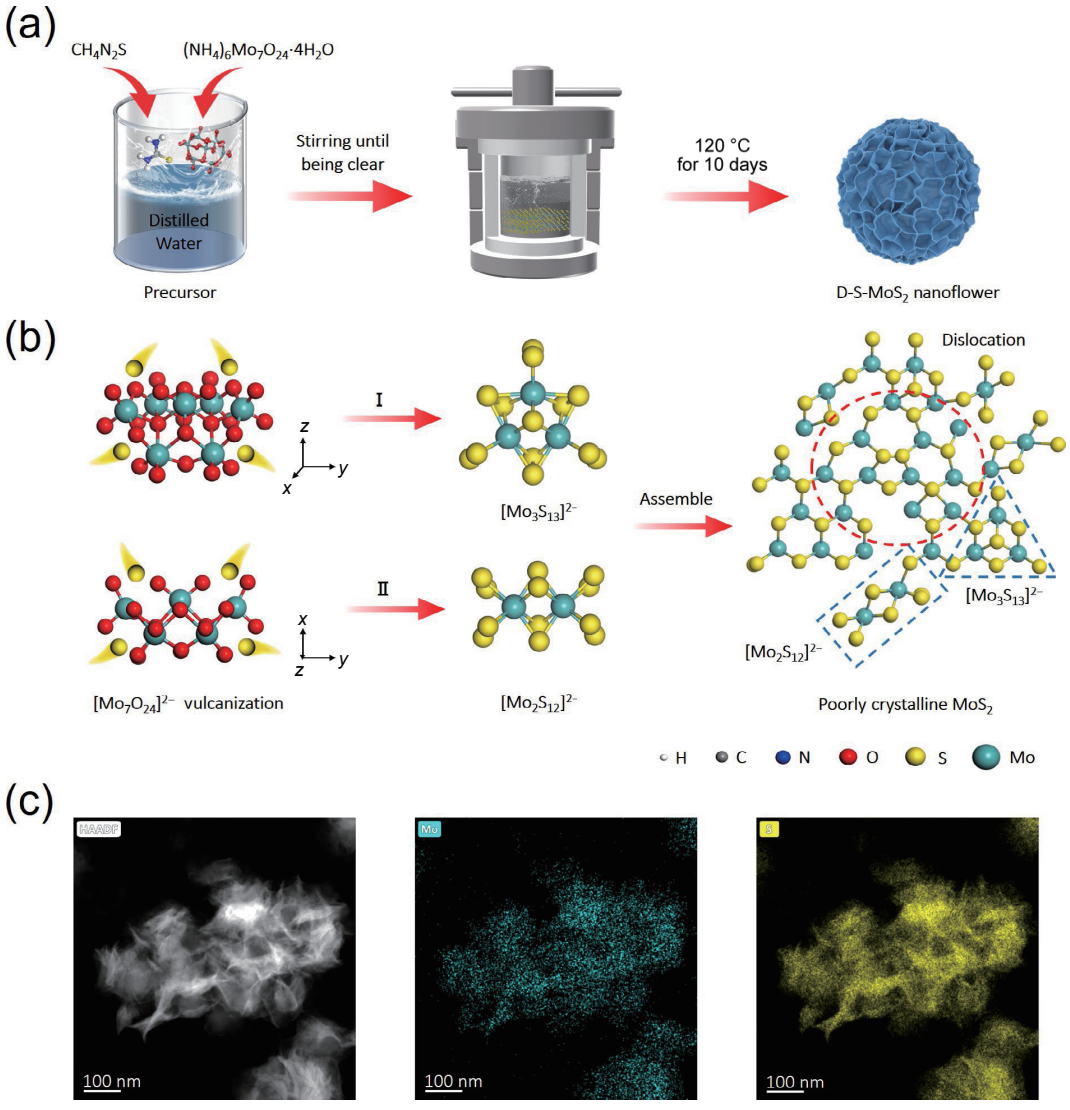

Figure 2 Process and principle of synthesis of disorder MoS_2 by hydrothermal method. (a) Schematic diagram of synthetic high-density dislocation intrinsic flexible MoS_2 nanosheets. (b) Schematic diagram of low temperature hydrothermal processing. (c) HRTEM image and corresponding EDX element mapping images of D-S-MoS_2 nanosheet, displaying the homogeneous distribution of Mo and S.

moiré pattern, which may be ascribed to the mechanical instability triggering the S-Mo-S layer sliding with the generation of dislocation (Fig. S7 in the ESM) [39, 49, 50]. Furthermore, the 100 and 101 crystal phases were separated by inverse fast Fourier transform (IFFT) and the corresponding in-plane dislocation information is displayed in Figs. 3(c) and 3(e) respectively. From Figs. 3(d) and 3(f), the strain is distributed in the corresponding lattice plane. In order to describe the strain field on the MoS_2 surface, the GPA method was used to obtain strain distribution images from HRTEM images. The GPA measurement was realized by strain ++ software [51]. The measurement applied to all HRTEM images and can adapt to different noise levels and misalignment. The HRTEM image and GPA analysis evidence that numerous dislocations will be generated after a low long-time hydrothermal process at low temperature, which will bring strain to the MoS_2 nanosheets, as exhibited in Figs. 3(d) and 3(f). The GPA image of the MoS_2 nanosheet suggests the compression–stretch dislocation dipole. As can be seen from Figs. 3(c) and 3(e), strain can be observed in the area containing a large number of dislocations, and these dislocations are indicated by "T". In addition, dislocations in one crystal phase may cause strain effects in another crystal phase, which does not contain dislocations in the same area and is marked with a white square.

To explore the electronic structure of D-S-MoS_2, X-ray photoelectron spectroscopy (XPS) was further used to track the movement of the Mo 3d peak on the MoS_2 nanosheet (Fig. S8 in the ESM). For the original 2H-MoS_2, the signals of Mo $3d_{5/2}$ and Mo $3d_{3/2}$ are detected at 229.7 and 232.8 eV, respectively, which belong to Mo^{4+}, while the signal at 226.9 eV is attributed to S 2s electrons [52]. As demonstrated in Fig. S8 in ESM, compared with 2H-MoS_2, the three main peak shapes of D-S-MoS_2 remain the same, except for the overall transfer to lower binding energy (~ 0.2 eV), indicating that the electron density around Mo atoms has increased. In addition, the structure of the S 2p peak has also changed, displaying an overall positive shift (~ 0.4 eV) compared with 2H-MoS_2 (Fig. S9 in the ESM) [53]. Due to the different electronegativity of atoms, the degree of displacement of its Mo 3d peak depends on the specific element (S) on its surface. Therefore, by introducing dislocations in MoS_2, the surface electron distribution of S was optimized. The results illustrate that the change of the electronic structure of the S atom will affect the adsorption/desorption energy of the reaction intermediate in the catalytic reaction, thereby affecting the catalytic activity. The XPS results indicate that the atomic ratio of Mo and S in D-S-MoS_2 is lower than 1:2, which is consistent with the EDX analysis.

In this work, the synthesized D-S-MoS_2 not only has a dislocation structure on the in-plane but also shows a dislocation structure out of the plane. The model image visually shows the

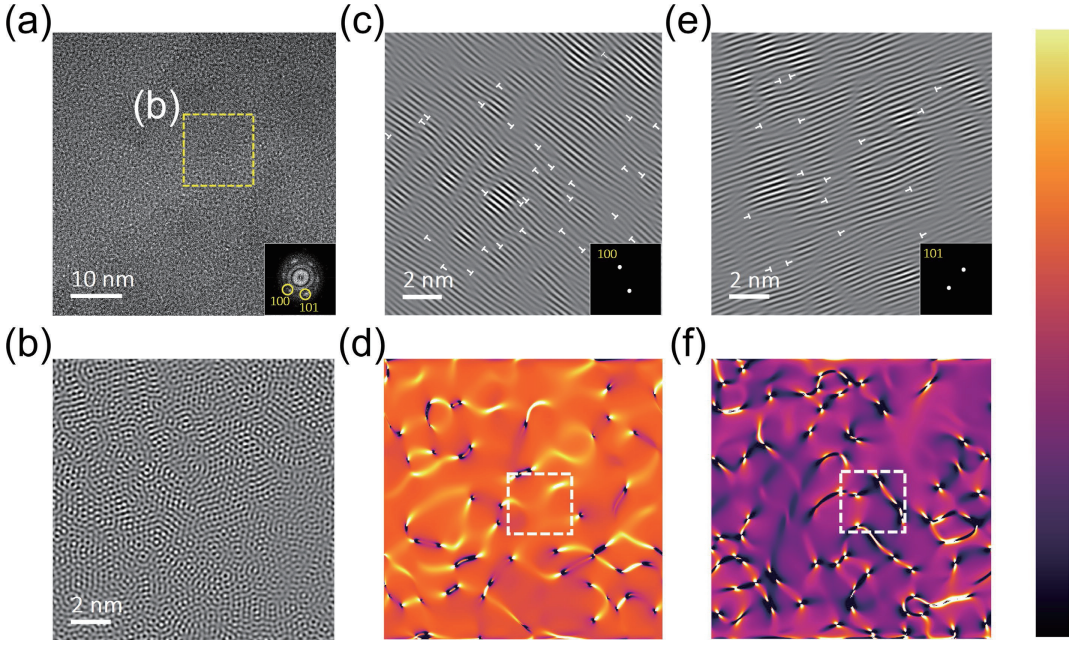

Figure 3 Analysis of D-S-MoS_2 in-plane strain caused by dislocation. (a) HRTEM image of the dislocation-strained MoS_2 nanosheets. (b) D-S-MoS_2 base image filtered by FFT in the yellow box area in (a). (c) and (e) The (100) and (101) crystal phase images containing numerous dislocations obtained by IFFT processing, in which the dislocations are represented by "T". (d) and (f) Strain distribution images of ε_{xy} and ε_{yy}, corresponding to (100) and (101) crystal phases, respectively. (Tensile strain is represented by brown to bright yellow, while compressive strain is represented by orange to dark purple.)

inherent flexibility of strain MoS_2 with out-of-plane dislocations (Fig. 4(a)). Figure 4(b) illustrates the formation mechanism of out-of-plane dislocations. The strain caused by dislocation induces bulges or depressions on the surface of MoS_2 nanosheets, resulting in interlayer lattice distortion and a large Burgers vector, resulting in atomic slip to form out of plane dislocations. Figure 4(c) shows a side view of the HRTEM of stacked D-S-MoS_2 nanosheets. Figure 4(d) displays D-S-MoS_2 has an extraordinary Zigzag structure (S-Mo-S-Mo-S multilayer sandwich structure). Due to the weak interlayer electronic coupling of MoS_2, the vertical conductivity is several orders of magnitude lower than the transverse conductivity, which would limit the inherent catalytic performance of the catalyst. Previous reports have shown that different layers can be connected by constructing dislocation defects, and the vertical transport can be transformed into transverse transport in the base plane to improve the vertical conductivity [31]. Dislocations form a large-scale interconnection network between MoS_2 layers so that electrons can easily flee in this out-of-plane dislocation structure, which makes the catalytic performance develop in a beneficial direction. Figure 4(e) indicates the GPA analysis of the D-S-MoS_2 dislocation network, with color mutations indicating that local strain tensors are induced. Specifically, the formation of out-of-plane dislocations promotes the non-parallel distribution between layers, and the interlayer van

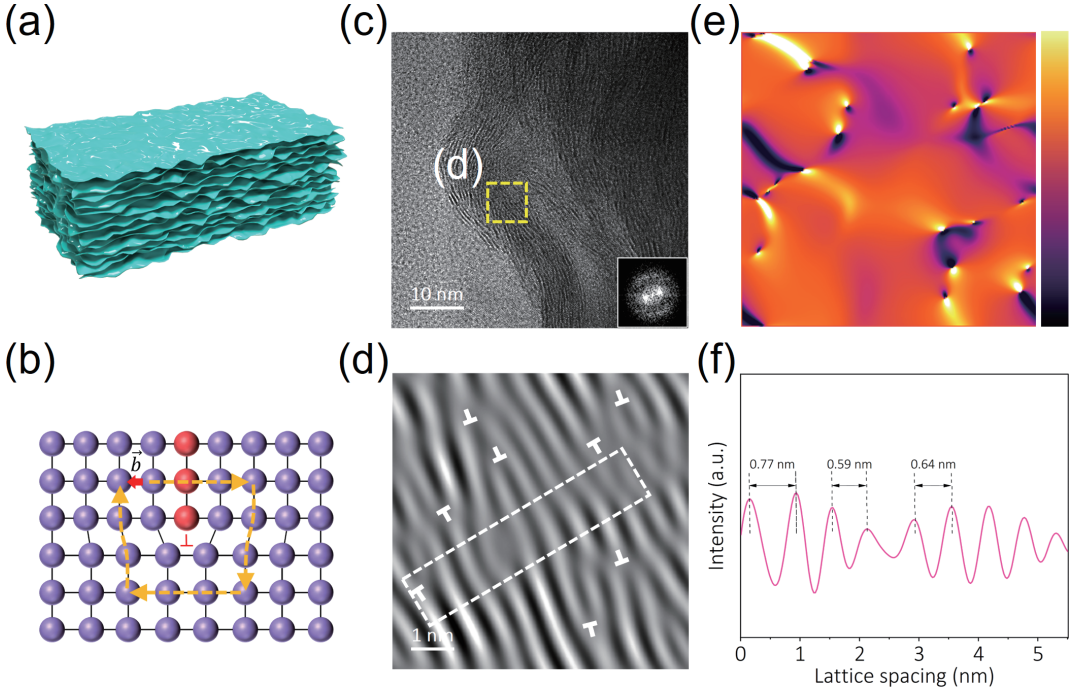

Figure 4 Analysis of D-S-MoS_2 interlayer strain caused by out-of-plane dislocations. (a) Schematic diagram of stacked flexible MoS_2 nanosheets with interlayer dislocation. (b) Schematic illustration of edge dislocations. (c) HRTEM image of the dislocation-strained MoS_2 nanosheets. (d) The corresponding FFT pattern in the region of the yellow box in (c). (e) Strain distributions of ε_{yy}, corresponding to the interlayer. (f) Line profile of the HRTEM image (white frame).

der Waals force changes, resulting in the expansion of one part of the interlayer spacing and the compression of the other part (Fig. 4(f)). In conclusion, distortion is a basic plastic deformation mode in layered materials with weak interlayer adhesion. This contributes to the change of layer spacing, and multi-layer splicing between MoS_2 layers may occur, which directly affects the state of electron transport between layers, to further improve the HER performance of the catalyst.

We evaluated the HER performance of the photocatalyst under visible light irradiation, and used Eosin Y (EY) and triethanolamine (TEOA) as sensitizers and sacrificial electron donors, respectively. It can be seen from Fig. 5(a) that the generated H_2 increases linearly with the irradiation time. The linearly increasing HER rate indicates remarkable stability, which can be attributed to the formation of high-density dislocations. The high-energy surface structure induced by strain can effectively resist the severe surface reconstruction in the catalytic reaction, thus improving the stability of the catalyst in the catalytic process. After 25 h, the HER rate decreases slightly, which may be caused by the consumption of EY. Figure S10 in the ESM displays the time courses of photocatalytic H_2 evolution over 2H-MoS_2. Interestingly, under the same experimental conditions, the HER rate of 2H-MoS_2 decreases significantly in about 3 h and reaches saturation in about 6 h. Previous studies have shown that the reason for the saturation of the HER rate is attributed to the depletion of protons and H^+ needs to be added to restart the reaction [54, 55]. Compared with 2H-MoS_2, D-S-MoS_2 can maintain a stable HER rate for a long time, indicating an extraordinary proton supply capacity. D-S-MoS_2 provides a large amount of H^+ for the reaction by splitting water, thereby promoting the HER. In addition, Fig. 5(b) compares the HER performance of MoS_2 synthesized at low temperatures in different periods. Under the same experimental conditions, D-S-MoS_2 synthesized in 10 days displays a champion HER activity. The HER performance of MoS_2 synthesized for 12 days shows a state of decay, which may be because that the better crystallinity causes a decrease in the number of active sites. Table S1 in the ESM lists the H_2 generation activity of MoS_2-based photocatalysts reported in recent years, demonstrating the efficient HER catalytic performance of D-S-MoS_2. The electron transfer process of D-S-MoS_2 under visible light irradiation is shown in Fig. 5(c). The reaction is photo-excited by EY to produce a triplet excited state (EY^{3*}). Electrons are obtained from TEOA by reductive quenching to produce free radical EY^-. Highly reductive EY^- can easily transfer electrons to protons to form excited H^* and collide with H adsorbed on the surface of D-S-MoS_2 to form H_2 [56].

To visually clarify the synergistic effect of dislocation and strain on their properties, DFT was used to calculate hydrogen adsorption free energy (ΔG_{H^*}) as a descriptor for correlating theoretical evaluation with experimental measurements of catalytic activity. From the perspective of thermodynamics, the ideal value of Gibbs free energy of hydrogen adsorption is 0 eV. The strong or weak adsorption of hydrogen on the active site will lead to the slow progress of electron transfer/proton reduction process. According to the magnitude of the strain field, H atom adsorption sites are constructed, as shown in Fig. 6(a). The strain effect caused by dislocations is manifested in the stretching and compression of the crystal lattice. Due to the existence of the dislocation nucleus, the surrounding Mo–Mo bonds have been compressed to varying degrees. Compared with the Mo?Mo bond length of 2H-MoS_2 (3.18 Å), the presence of high-density dislocations leads to 0.1%–4% compression of the lattice, which is consistent with the GPA results. Figure 6(b) shows the ΔG_{H^*} on the MoS_2 surface affected by the strain field and dislocation defects. The in-plane of pristine 2H-MoS_2 shows a high ΔG_{H^*} (~ 2.2 eV). The ΔG_{H^*} of D-S-MoS_2 with a lattice compression of 0.1% is about 0.42 eV, while the ΔG_{H^*} could be optimized to be −0.18 eV when the lattice compression is 4%. Theories and experiments have confirmed that the dislocation–strain synergistic strategy is indeed the key factor to improving the catalytic activity.

Therefore, the high-efficiency HER activity can be attributed to the below reasons. On one hand, the dislocation with the strain effect can fine-tune the electronic structure of the active site by moving the d-band center of the S atom down to the Fermi level,

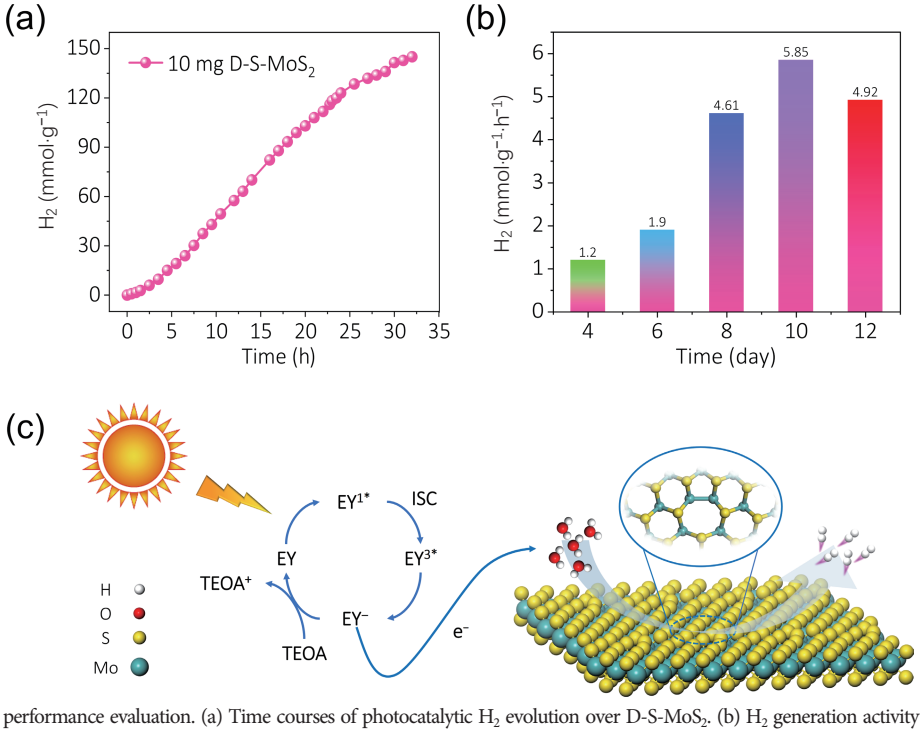

Figure 5 Photocatalytic performance evaluation. (a) Time courses of photocatalytic H_2 evolution over D-S-MoS_2. (b) H_2 generation activity values of D-S-MoS_2 and the pristine MoS_2 (light source: 300 W Xe lamp, λ: 350–760 nm, and irradiation area: 44.2 cm^2 reactor). (c) High-efficiency HER mechanism of D-S-MoS_2 in practical photocatalytic reaction.

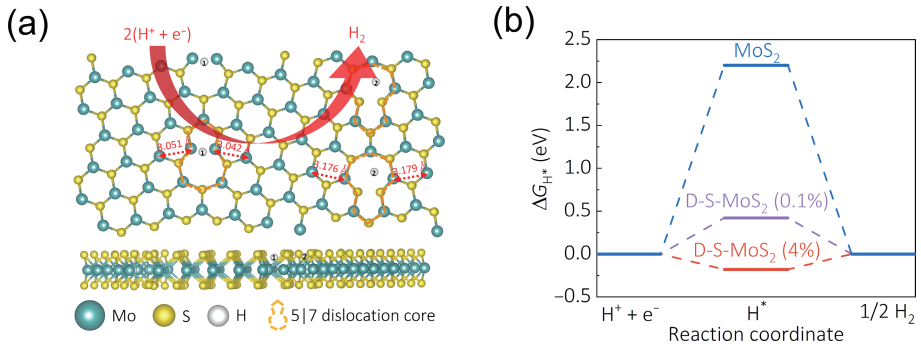

Figure 6 Theoretical calculation research on HER performance of D-S-MoS_2. (a) The schematic diagram of the top view (above) and side view (below) of MoS_2. (b) Gibbs free energies of D-S-MoS_2 at different lattice compressibilities.

which allows ΔG_{H^*} close to zero, thus improving the HER performance. On the other hand, the resulting stacking fault can connect interlayers and provide an electron transfer network to ensure the vertical conductivity for better HER activity.

3 Results and discussion

In summary, we report a low-temperature hydrothermal method for synthesizing strained MoS_2 nanosheets with in-plane and out-of-plane dislocations. It is worth emphasizing that the synthesized D-S-MoS_2 exhibits extraordinary HER activity in a homogenous dye-sensitized photocatalysis reaction. The D-S-MoS_2 presents fabulous HER photocatalytic activity attaining H_2 generation activity of 5.85 $mmol \cdot g^{-1} \cdot h^{-1}$ with outstanding stability under the irradiation of a 300 W Xe lamp. In addition, DFT results reveal that the strain induced by dislocation could manipulate the hydrogen adsorption free energy to optimize the HER activity. The underlying relationship between structure, properties, and performance of D-S-MoS_2 for improving photocatalytic HER activity is established clearly. This work provides a new method for exploring and building a high-performance photocatalytic hydrogen production system by dislocation engineering.

Acknowledgements

This work was financially supported by the National Funds for Distinguished Young Scientists (No. 61825503), the National Natural Science Foundation of China (Nos. 51902101, 61775101, and 61804082), the Youth Natural Science Foundation of Hunan Province (No. 2021JJ40044), the Natural Science Foundation of Jiangsu Province (No. BK20201381), and the Science Foundation of Nanjing University of Posts and Telecommunications (No. NY219144).

Electronic Supplementary Material: Supplementary material (XPS, HRTEM, scanning electron microscopy (SEM), XRD, ESR, EDS spectrum diagram, Xenon lamp spectrum, D-S-MoS_2 synthesis method, photocatalytic experiment method, and theoretical calculation method) is available in the online version of this article at https://doi.org/10.1007/s12274-022-4158-0.

References

[1] Stamenkovic, V. R.; Fowler, B.; Mun, B. S.; Wang, G. F.; Ross, P. N.; Lucas, C. A.; Marković, N. M. Improved oxygen reduction activity on $Pt_3Ni(111)$ via increased surface site availability. *Science* **2007**, *315*, 493–497.

[2] Wang, X.; Zhang, Y. W.; Si, H. N.; Zhang, Q. H.; Wu, J.; Gao, L.; Wei, X. F.; Sun, Y.; Liao, Q. L.; Zhang, Z. et al. Single-atom vacancy defect to trigger high-efficiency hydrogen evolution of MoS_2. *J. Am. Chem. Soc.* **2020**, *142*, 4298–4308.

[3] Li, H.; Tsai, C.; Koh, A. L.; Cai, L. L.; Contryman, A. W.; Fragapane, A. H.; Zhao, J. H.; Han, H. S.; Manoharan, H. C.; Abild-Pedersen, F. et al. Activating and optimizing MoS_2 basal planes for hydrogen evolution through the formation of strained sulphur vacancies. *Nat. Mater.* **2016**, *15*, 48–53.

[4] Zheng, Z. L.; Yu, L.; Gao, M.; Chen, X. Y.; Zhou, W.; Ma, C.; Wu, L. H.; Zhu, J. F.; Meng, X. Y.; Hu, J. T. et al. Boosting hydrogen evolution on MoS_2 via co-confining selenium in surface and cobalt in inner layer. *Nat. Commun.* **2020**, *11*, 3315.

[5] Han, A.; Zhou, X. F.; Wang, X. J.; Liu, S.; Xiong, Q. H.; Zhang, Q. H.; Gu, L.; Zhuang, Z. C.; Zhang, W. J.; Li, F. X. et al. One-step synthesis of single-site vanadium substitution in 1T-WS_2 monolayers for enhanced hydrogen evolution catalysis. *Nat. Commun.* **2021**, *12*, 709.

[6] Zhang, J.; Wu, J. J.; Guo, H.; Chen, W. B.; Yuan, J. T.; Martinez, U.; Gupta, G.; Mohite, A.; Ajayan, P. M.; Lou, J. Unveiling active sites for the hydrogen evolution reaction on monolayer MoS_2. *Adv. Mater.* **2017**, *29*, 1701955.

[7] Ye, G. L.; Gong, Y. J.; Lin, J. H.; Li, B.; He, Y. M.; Pantelides, S. T.; Zhou, W.; Vajtai, R.; Ajayan, P. M. Defects engineered monolayer MoS_2 for improved hydrogen evolution reaction. *Nano Lett.* **2016**, *16*, 1097–1103.

[8] Li, G. Q.; Zhang, D.; Qiao, Q.; Yu, Y. F.; Peterson, D.; Zafar, A.; Kumar, R.; Curtarolo, S.; Hunte, F.; Shannon, S. et al. All the catalytic active sites of MoS_2 for hydrogen evolution. *J. Am. Chem. Soc.* **2016**, *138*, 16632–16638.

[9] Zhou, G.; Shan, Y.; Wang, L. L.; Hu, Y. Y.; Guo, J. H.; Hu, F. R.; Shen, J. C.; Gu, Y.; Cui, J. T.; Liu, L. Z. et al. Photoinduced semiconductor-metal transition in ultrathin troilite FeS nanosheets to trigger efficient hydrogen evolution. *Nat. Commun.* **2019**, *10*, 399.

[10] Rao, F.; Zhu, G. Q.; Zhang, W. B.; Gao, J. Z.; Zhang, F. C.; Huang, Y.; Hojamberdiev, M. *In-situ* generation of oxygen vacancies and metallic bismuth from $(BiO)_2CO_3$ via N_2-assisted thermal-treatment for efficient selective photocatalytic NO removal. *Appl. Catal. B:Environ.* **2021**, *281*, 119481.

[11] Li, Y.; Wang, Q. Z.; Hu, X. S.; Meng, Y.; She, H. D.; Wang, L.; Huang, J. W.; Zhu, G. Q. Constructing NiFe-metal-organic frameworks from NiFe-layered double hydroxide as a highly efficient cocatalyst for $BiVO_4$ photoanode PEC water splitting. *Chem. Eng. J.*, in press, DOI: https://doi.org/10.1016/j.cej.2021.133592.

[12] Voiry, D.; Fullon, R.; Yang, J.; de Carvalho Castro, E. Silva C.; Kappera, R.; Bozkurt, I.; Kaplan, D.; Lagos, M. J.; Batson, P. E.; Gupta, G. et al. The role of electronic coupling between substrate and 2D MoS_2 nanosheets in electrocatalytic production of hydrogen. *Nat. Mater.* **2016**, *15*, 1003–1009.

[13] Sun, T.; Wang, J.; Chi, X.; Lin, Y. X.; Chen, Z. X.; Ling, X.; Qiu, C. T.; Xu, Y. S.; Song, L.; Chen, W. et al. Engineering the electronic structure of MoS_2 nanorods by N and Mn dopants for ultra-efficient hydrogen production. *ACS Catal.* **2018**, *8*, 7585–7592.

[14] Zhuang, Z. C.; Li, Y.; Huang, J. Z.; Li, Z. L.; Zhao, K. N.; Zhao, Y. L.; Xu, L.; Zhou, L.; Moskaleva, L. V.; Mai, L. Q. *Sisyphus* effects in hydrogen electrochemistry on metal silicides enabled by silicene subunit edge. *Sci. Bull.* **2019**, *64*, 617–624.

[15] Chen, Y.; Huang, S. X.; Ji, X.; Adepalli, K.; Yin, K. D.; Ling, X.; Wang, X. W.; Xue, J. M.; Dresselhaus, M.; Kong, J. et al. Tuning

electronic structure of single layer MoS_2 through defect and interface engineering. *ACS Nano* **2018**, *12*, 2569–2579.
[16] Wang, Y.; Zheng, X. B.; Wang, D. S. Design concept for electrocatalysts. *Nano Res*., in press, DOI: https://doi.org/10.1007/s12274-021-3794-0.
[17] Liu, Z. H.; Du, Y.; Zhang, P. F.; Zhuang, Z. C.; Wang, D. S. Bringing catalytic order out of chaos with nitrogen-doped ordered mesoporous carbon. *Matter* **2021**, *4*, 3161–3194.
[18] Wang, H. Q.; Zhang, W. J.; Zhang, X. W.; Hu, S. X.; Zhang, Z. C.; Zhou, W. J.; Liu, H. Multi-interface collaboration of graphene cross-linked NiS-NiS_2-Ni_3S_4 polymorph foam towards robust hydrogen evolution in alkaline electrolyte. *Nano Res.* **2021**, *14*, 4857–4864.
[19] Ouyang, Y. X.; Ling, C. Y.; Chen, Q.; Wang, Z. L.; Shi, L.; Wang, J. L. Activating inert basal planes of MoS_2 for hydrogen evolution reaction through the formation of different intrinsic defects. *Chem. Mater.* **2016**, *28*, 4390–4396.
[20] He, Y. M.; Tang, P. Y.; Hu, Z. L.; He, Q. Y.; Zhu, C.; Wang, L. Q.; Zeng, Q. S.; Golani, P.; Gao, G. H.; Fu, W. et al. Engineering grain boundaries at the 2D limit for the hydrogen evolution reaction. *Nat. Commun.* **2020**, *11*, 57.
[21] Gao, L.; Liao, Q. L.; Zhang, X. K.; Liu, X. Z.; Gu, L.; Liu, B. S.; Du, J. L.; Ou, Y.; Xiao, J. K.; Kang, Z. et al. Defect-engineered atomically thin MoS_2 homogeneous electronics for logic inverters. *Adv. Mater.* **2020**, *32*, 1906646.
[22] Jiang, Z. M.; Pikul, J. H. Centimetre-scale crack-free self-assembly for ultra-high tensile strength metallic nanolattices. *Nat. Mater.* **2021**, *20*, 1512–1518.
[23] Kibsgaard, J.; Chen, Z. B.; Reinecke, B. N.; Jaramillo, T. F. Engineering the surface structure of MoS_2 to preferentially expose active edge sites for electrocatalysis. *Nat. Mater.* **2012**, *11*, 963–969.
[24] Cao, P. Q.; Wu, J. Y. Self-assembly of MoS_2 monolayer sheets by desulfurization. *Langmuir* **2021**, *37*, 4971–4983.
[25] Xie, W. H.; Wei, Y. J. Roughening for strengthening and toughening in monolayer carbon based composites. *Nano Lett.* **2021**, *21*, 4823–4829.
[26] Maiti, S.; Maiti, K.; Curnan, M. T.; Kim, K.; Noh, K. J.; Han, J. W. Engineering electrocatalyst nanosurfaces to enrich the activity by inducing lattice strain. *Energy Environ. Sci.* **2021**, *14*, 3717–3756.
[27] Chen, Y. C.; Lu, A. Y.; Lu, P.; Yang, X. L.; Jiang, C. M.; Mariano, M.; Kaehr, B.; Lin, O.; Taylor, A.; Sharp, I. D. et al. Structurally deformed MoS_2 for electrochemically stable, thermally resistant, and highly efficient hydrogen evolution reaction. *Adv. Mater.* **2017**, *29*, 1703863.
[28] Ding, Q.; Song, B.; Xu, P.; Jin, S. Efficient electrocatalytic and photoelectrochemical hydrogen generation using MoS_2 and related compounds. *Chem* **2016**, *1*, 699–726.
[29] Zhuang, Z. C.; Li, Y.; Li, Y. H.; Huang, J. Z.; Wei, B.; Sun, R.; Ren, Y. J.; Ding, J.; Zhu, J. X.; Lang, Z. Q. et al. Atomically dispersed nonmagnetic electron traps improve oxygen reduction activity of perovskite oxides. *Energy Environ. Sci.* **2021**, *14*, 1016–1028.
[30] Fu, Y.; Shan, Y.; Zhou, G.; Long, L. Y.; Wang, L. L.; Yin, K. B.; Guo, J. H.; Shen, J. C.; Liu, L. Z.; Wu, X. L. Electric strain in dual metal janus nanosheets induces structural phase transition for efficient hydrogen evolution. *Joule* **2019**, *3*, 2955–2967.
[31] Laursen, A. B.; Kegnæs, S.; Dahl, S.; Chorkendorff, I. Molybdenum sulfides-efficient and viable materials for electro-and photoelectrocatalytic hydrogen evolution. *Energy Environ. Sci.* **2012**, *5*, 5577–5591.
[32] Huang, T. X.; Cong, X.; Wu, S. S.; Lin, K. Q.; Yao, X.; He, Y. H.; Wu, J. B.; Bao, Y. F.; Huang, S. C.; Wang, X. et al. Probing the edge-related properties of atomically thin MoS_2 at nanoscale. *Nat. Commun.* **2019**, *10*, 5544.
[33] Tong, X. P.; Zhao, Y.; Zhuo, Z. W.; Yang, Z. H.; Wang, S. Z.; Liu, Y. W.; Lu, N.; Li, H. Q.; Zhai, T. Y. Dual-regulation of defect sites and vertical conduction by spiral domain for electrocatalytic hydrogen evolution. *Angew. Chem., Int. Ed.*, in press, DOI: https://doi.org/10.1002/anie.202112953.
[34] Wu, J. Y.; Gong, H.; Zhang, Z. S.; He, J. Y.; Ariza, P.; Ortiz, M.; Zhang, Z. L. Topology and polarity of dislocation cores dictate the mechanical strength of monolayer MoS_2. *Appl. Mater. Today* **2019**, *15*, 34–42.
[35] Wu, J. Y.; Cao, P. Q.; Zhang, Z. S.; Ning, F. L.; Zheng, S. S.; He, J. Y.; Zhang, Z. L. Grain-size-controlled mechanical properties of polycrystalline monolayer MoS_2. *Nano Lett.* **2018**, *18*, 1543–1552.
[36] Lin, J. H.; Pantelides, S. T.; Zhou, W. Vacancy-induced formation and growth of inversion domains in transition-metal dichalcogenide monolayer. *ACS Nano* **2015**, *9*, 5189–5197.
[37] Zhu, J. Q.; Wang, Z. C.; Dai, H. J.; Wang, Q. Q.; Yang, R.; Yu, H.; Liao, M. Z.; Zhang, J.; Chen, W.; Wei, Z. et al. Boundary activated hydrogen evolution reaction on monolayer MoS_2. *Nat. Commun.* **2019**, *10*, 1348.
[38] Zou, X. L.; Liu, Y. Y.; Yakobson, B. I. Predicting dislocations and grain boundaries in two-dimensional metal-disulfides from the first principles. *Nano Lett.* **2013**, *13*, 253–258.
[39] Bertoldo, F.; Unocic, R. R.; Lin, Y. C.; Sang, X. H.; Puretzky, A. A.; Yu, Y. L.; Miakota, D.; Rouleau, C. M.; Schou, J.; Thygesen, K. S. et al. Intrinsic defects in MoS_2 grown by pulsed laser deposition: From monolayers to bilayers. *ACS Nano* **2021**, *15*, 2858–2868.
[40] Wang, L. L.; Xie, L. B.; Zhao, W. W.; Liu, S. J.; Zhao, Q. Oxygen-facilitated dynamic active-site generation on strained MoS_2 during photo-catalytic hydrogen evolution. *Chem. Eng. J.* **2021**, *405*, 127028.
[41] Xie, J. F.; Zhang, J. J.; Li, S.; Grote, F.; Zhang, X. D.; Zhang, H.; Wang, R. X.; Lei, Y.; Pan, B. C.; Xie, Y. Controllable disorder engineering in oxygen-incorporated MoS_2 ultrathin nanosheets for efficient hydrogen evolution. *J. Am. Chem. Soc.* **2013**, *135*, 17881–17888.
[42] Liu, S. L.; Hu, Z.; Wu, Y. Z.; Zhang, J. F.; Zhang, Y.; Cui, B. H.; Liu, C.; Hu, S.; Zhao, N. Q.; Han, X. P. et al. Dislocation-strained IrNi alloy nanoparticles driven by thermal shock for the hydrogen evolution reaction. *Adv. Mater.* **2020**, *32*, 2006034.
[43] Ronge, E.; Hildebrandt, S.; Grutza, M. L.; Klein, H.; Kurz, P.; Jooss, C. Structure of nanocrystalline, partially disordered $MoS_{2+\delta}$ derived from HRTEM—an abundant material for efficient HER catalysis. *Catalysts* **2020**, *10*, 856.
[44] Yin, Y.; Zhang, Y. M.; Gao, T. L.; Yao, T.; Zhang, X. H.; Han, J. C.; Wang, X. J.; Zhang, Z. H.; Xu, P.; Zhang, P. et al. Synergistic phase and disorder engineering in 1T-$MoSe_2$ nanosheets for enhanced hydrogen-evolution reaction. *Adv. Mater.* **2017**, *29*, 1700311.
[45] Ye, S. H.; Wang, J. P.; Hu, J.; Chen, Z. D.; Zheng, L. R.; Fu, Y. H.; Lei, Y. Q.; Ren, X. Z.; He, C. X.; Zhang, Q. L. et al. Electrochemical construction of low-crystalline CoOOH nanosheets with short-range ordered grains to improve oxygen evolution activity. *ACS Catal.* **2021**, *11*, 6104–6112.
[46] Chen, X. F.; Wang, Q.; Cheng, Z. Y.; Zhu, M. L.; Zhou, H.; Jiang, P.; Zhou, L. L.; Xue, Q. Q.; Yuan, F. P.; Zhu, J. et al. Direct observation of chemical short-range order in a medium-entropy alloy. *Nature* **2021**, *592*, 712–716.
[47] Dai, Z. H.; Liu, L. Q.; Zhang, Z. Strain engineering of 2D materials: Issues and opportunities at the interface. *Adv. Mater.* **2019**, *31*, 1805417.
[48] Liu, Z.; Amani, M.; Najmaei, S.; Xu, Q.; Zou, X. L.; Zhou, W.; Yu, T.; Qiu, C. Y.; Birdwell, A. G.; Crowne, F. J. et al. Strain and structure heterogeneity in MoS_2 atomic layers grown by chemical vapour deposition. *Nat. Commun.* **2014**, *5*, 5246.
[49] Ly, T. H.; Perello, D. J.; Zhao, J.; Deng, Q. M.; Kim, H.; Han, G. H.; Chae, S. H.; Jeong, H. Y.; Lee, Y. H. Misorientation-angle-dependent electrical transport across molybdenum disulfide grain boundaries. *Nat. Commun.* **2016**, *7*, 10426.
[50] Xie, L. B.; Wang, L. L.; Zhao, W. W.; Liu, S. J.; Huang, W.; Zhao, Q. WS_2 moiré superlattices derived from mechanical flexibility for hydrogen evolution reaction. *Nat. Commun.* **2021**, *12*, 5070.
[51] Hÿtch, M. J.; Snoeck, E.; Kilaas, R. Quantitative measurement of displacement and strain fields from HREM micrographs. *Ultramicroscopy* **1998**, *74*, 131–146.
[52] Li, L.; Qin, Z. D.; Ries, L.; Hong, S.; Michel, T.; Yang, J.; Salameh, C.; Bechelany, M.; Miele, P.; Kaplan, D. et al. Role of sulfur vacancies and undercoordinated Mo regions in MoS_2 nanosheets toward the evolution of hydrogen. *ACS Nano* **2019**, *13*, 6824–6834.
[53] Liu, W.; Xu, Q.; Cui, W. L.; Zhu, C. H.; Qi, Y. H. CO_2-assisted

fabrication of two-dimensional amorphous molybdenum oxide nanosheets for enhanced plasmon resonances. *Angew. Chem., Int. Ed.* **2017**, *56*, 1600–1604.

[54] Chou, S. S.; Sai, N.; Lu, P.; Coker, E. N.; Liu, S.; Artyushkova, K.; Luk, T. S.; Kaehr, B.; Brinker, C. J. Understanding catalysis in a multiphasic two-dimensional transition metal dichalcogenide. *Nat. Commun.* **2015**, *6*, 8311.

[55] Maitra, U.; Gupta, U.; De, M.; Datta, R.; Govindaraj, A.; Rao, C. N. R. Highly effective visible-light-induced H_2 generation by single-layer 1T-MoS_2 and a nanocomposite of few-layer 2H-MoS_2 with heavily nitrogenated graphene. *Angew. Chem., Int. Ed.* **2013**, *52*, 13057–13061.

[56] Du, P. W.; Schneider, J.; Jarosz, P.; Eisenberg, R. Photocatalytic generation of hydrogen from water using a platinum(II) terpyridyl acetylide chromophore. *J. Am. Chem. Soc.* **2006**, *128*, 7726–7727.